Effect of plasma irradiation on biocompatibility and cell adhesion of polyaniline / chitosan nanocomposites towards Hep G$_2$ and PBMC cells

Ashok Kumar*, Rajiv Borah

Materials Research Laboratory, Department of Physics, Tezpur University, Tezpur, 784028, India

*Corresponding author, E-mail: ask@tezu.ernet.in; Tel: (+91) 3712275553

Abstract

Surface modification of polymeric biomaterials for tissue engineering applications has drawn considerable research interest. In this work, the surface of polyaniline (PAni) nanofibers/chitosan nanocomposites has been modified by plasma irradiation technique to improve its biocompatibility. The average diameter of PAni nanofibers determined by HRTEM is 35.66 nm, whereas FESEM images depict interconnected network of nanofibers dispersed uniformly throughout the chitosan matrix. XRD patterns of PAni/Chitosan nanocomposites after plasma treatment indicate increase in amorphous nature. The alterations in surface morphology after plasma treatment have been confirmed with the help of SEM analysis. The surface chemistry of the samples after plasma treatment has been investigated by means of ATR-FTIR and contact angle measurements. The ATR-FTIR spectra and surface energy measurements show incorporation of polar functional groups after oxygen (O$_2$) and nitrogen (N$_2$) plasma treatment. Preliminary biocompatibility assessments of the plasma treated PAni/Chitosan nanocomposites have been accomplished using Alamar Blue assay with Hep G$_2$ and Primary peripheral blood mononuclear (PBMC) cells. Both assays show maximum enhancement in cell viability for O$_2$ and N$_2$ plasma treated samples, comparing to the pristine one, whereas least cell viability was observed for Ar plasma treated samples. This study depicts that gas plasma treatment can effectively enhance the bioactivity of PAni/Chitosan nanocomposites and can make them attractive for tissue engineering applications. Copyright © 2016 VBRI Press.

Keywords: Surface modification, biomaterials, plasma irradiation, biocompatibility, cell viability.

Introduction

Tissue and organ failure, caused due to injury or other types of damage, is a major challenge in health care across the world. With the recent advancement in medical science, there are options for treatment which include transplantation, surgical repair, artificial prostheses, mechanical devices and drug therapy. However, these methods can neither repair nor recover of a severely damaged tissue or organ in satisfactory way. Moreover, transplant rejection, during which the body has an immune response to the transplanted organ, possibly leading to transplant failure. A distinctive feature of tissue engineering is to regenerate patient's own tissues and organs that are entirely free of poor biocompatibility and low biofunctionality as well as severe immune rejection [1-3].

Tissue engineering, which focuses on regeneration of neotissues from cells with the support of biomaterials and growth factors, is emerging as a significant potential alternative or complementary solution, whereby tissue and organ failure is addressed by implanting natural, synthetic, or semi synthetic tissue and organ mimics that are fully functional from the start, or that grow into the required functionality. The fundamentals of tissue engineering involve the cell sources, scaffolds for cell expansion and differentiation and carriers for growth factors [1-5]. To fulfill the functions of a scaffold in tissue engineering, the scaffold should meet a number of requirements. First, it should be biocompatible and biodegradable and have interconnected micropores, so that numerous cells can be seeded, migrate into the inside, increase the cell number and should be supplied by sufficient amounts of nutrients. The absorption kinetics of scaffold material will profoundly affect the success rate of tissue engineering [1-5].

The scaffold should mimic the structure and biological function of native extracellular matrix (ECM) as much as possible, both in terms of

chemical composition and physical structure [4]. In spite of the amazing diversity of ECM structures caused by different biomacromolecules and the way they are organized, a well-known feature of native ECM is the nanoscaled dimensions of their physical structure. In a typical connective tissue, structural protein fibers such as collagen fibers and elastin fibers have diameters ranging from several ten to several hundred nanometers. Adhesive proteins such as fibronectin and laminin, which provide specific binding site for cell adhesion, also exist as nanoscaled fibers in ECM [7-8]. The fibers, pores, ridges, and grooves on the basement membrane are all nanoscaled, from several to more than 100 nm. Cells attach to and organize around fibers with diameters smaller than that of the cells [9]. Nanoscaled surface roughness with dimensions ranging from 20 to 50 nm produced by chemical etching on silicon wafers enhanced neural cell adhesion and hydroxylase activity [10] Nanoscaled surface topography has also been found to promote osteoblast adhesions [11]. One study reported that osteoblast adhesion, proliferation, alkaline phosphatase activity, and ECM secretion on carbon nanofibers increased with deceasing fiber diameter in the range of 60–200 nm, whereas the adhesion of other kinds of cells such as chondrocytes, fibroblasts, and smooth muscle cells was not influenced [12]. Polymeric nanofiber nonwoven matrix is among the most promising biomaterials for native ECM analogs [13].

Moreover, electroactive biomaterials as scaffolds allow direct delivery of electrical, electrochemical and electromechanical stimulation to cells [14]. Regarding the electrical properties of cells, electrical signals strongly affects cell behavior, affecting ion influx across the cell membrane, altering the membrane potential and conditioning the intracellular signal transduction pathways [15]. Thus, electrical charges and electrical fields have beneficial healing effects on various tissues, including bone, cartilage, skin and connective tissue, cranial and spinal nerves and peripheral nerves. Conducting polymers (CPs) allow excellent control of the electrical stimulus, possess very good electrical and optical properties, have a high conductivity/weight ratio and can be made biocompatible, biodegradable and porous [14] Furthermore, a great advantage of conductive polymers is that their chemical, electrical and physical properties can be tailored to the specific needs of their application by incorporating antibodies, enzymes and other biological moieties [14] Thus, strategies designed to enhance the regeneration of a responsive cell might employ electrically conducting polymers.

The most important parameter of cell biomaterials interaction through adsorption of proteins is the surface hydrophilicity, which in fact allows covalent attachment of proteins atop materials' surface and presents normal bioactivity to the biomolecules

[16,17]. On the other hand, CPs are often considered as synthetic hydrophobic materials. Therefore, it is necessary to increase the hydrophilicity of the surface of CPs. It can be achieved through incorporation of polar groups like hydroxyl, carboxylic, aldehyde, amino and sulphate groups atop materials' surface. The alteration of the presence and density of polar groups on the material's surface can be used to tailor its wettability and surface free energy and hence to adjust surface biocompatibility in accordance with the application [16, 17].

Plasma-surface modification is an effective and economical technique, applicable for many materials and of growing interest in the biomaterials field. The main advantage of plasma modification techniques is that the surface properties can be enhanced selectively, while the bulk attributes of the materials remain unchanged. Plasma based treatments have been largely used for medical applications with different aims, such as the introduction of new functionalities, enhancement of surface wettability, increase of the surface oxygen concentration and improvement of the interfacial adhesion [18-21] Depending on the conditions and the plasma species, the polymer surface properties such as hydrophobicity, morphology and the adhesion can be altered [22]. O_2 plasma is often used to impart oxygen containing functional groups to polymer surfaces such as PCL, PE and PET [18, 23-26]. N_2 plasma has been used to impart amine groups to the surface of PTFE and PS [18, 27, 28]. Inert gases can be used to introduce radical sites on the polymer surface.[18] Plasma technique has a major advantage over the conventional wet chemical process in terms of reduction of waste and pollution problems and conservation of chemicals, water, energy, and time.

Polyaniline (PAni) is one of the most mesmerizing CPs due to its diverse structural forms, ease of synthesis, high environmental stability and excellent charge transport property by doping/dedoping process. However, some serious issues like biocompatibility, biodegradability including unexpected side effects of bioactivity are of critical concern during biomedical application of these materials. Mattioli-Belmonte et al. were the first to demonstrate that this polymer is biocompatible in vitro and in vivo [29]. It has been reported PAni derivatives were found to be able to function as biocompatible substrates, upon which both H9c2 cardiac myoblasts and PC-12 pheochromocytoma cells can adhere, grow and differentiate well [30]. Recently, to overcome the poor biodegradability and biocompatibility, PAni has been blended with natural and synthetic biopolymers for various biomedical applications like tissue engineering [31, 32], biosensing [33], drug delivery [34] etc.

The subject matter of the present research includes synthesis and surface modification of bioactive and biodegradable 1D nanostructured electroactive conducting polymer based nanocomposites. Based on

the unique ability of CPs to respond to electrical or electromagnetic stimuli, they can act as an interface between the external and physiological environments of a connective tissue such as bone, which is capable of undergoing repair and regeneration on exposure to the same stimuli [15]. 1D CP nanostructures can be functionalized through incorporation of polar functional groups such as carboxyl, amino, hydroxyl groups onto their surface. Intrinsically biodegradable biomaterials can also be achieved by blending conducting polymer nanostructures with natural biopolymers such as collagen, chitosan and gelatin. There are only a few reports of proliferation of cancer cells on PAni based biomaterial so far [35]. and effect of gas plasma treatment on biocompatibility of PAni nanofibers/Chitosan nanocomposites has not been investigated yet. We are attempting here to modify the surface of PAni nanofibers/Chitosan nanocomposites by O_2, N_2 and Ar plasma treatment to study its effect on biocompatibility towards human liver hepatocellular carcinoma cell line (Hep G2) cells and peripheral human blood mononuclear cells (PBMC). Consequent effect of surface modification on surface hydrophilicity of the nanocomposites has been investigated with the help of attenuated total reflectance fourier transform (ATR-FTIR) spectroscopy and surface energy calculations using contact angle measurement along with the chemical mechanisms of incorporations of polar functionality after plasma surface modification. The results were correlated to the improved cell biomaterial interactions. This research is intended to make an attempt to explore the potential application oriented possibilities of surface modified nanostructured conducting polymer based materials as a scaffold for cancer cell growth for therapy as an alternative to the conventional metal based technologies.

Experimental

Materials

Aniline (p.a. Merck Germany, ≥99.5%) was distilled under reduced pressure before use. Ammonium peroxydisulfate (p.a. Merck Germany, ≥98%) and Hydrochloric acid (p.a. Sigma Aldrich, 37% AR grade) were used without further purification. Deionised water (12 MΩ cm) used for the synthesis was obtained from a Milli-Q system. Chitosan extrapure (p.a. SRL India, ≥99%) were as used as obtained. Acetic acid (p.a. Sigma Aldrich, ≥99.85%). All other chemicals and reagents were of analytical grade and used as received.

Analytical techniques

Transmission electron microscopy was accomplished using a JEOL JEM 200 CX transmission electron microscope (TEM) installed at SAIF, NEHU, Shillong. Morphological characterizations were carried out using Sigma VP G8 Advanced modeled scanning electron microscope at IASST, Guwahati, India before surface modification and JSM 6390LV

JEOL, JAPAN at Department of Physics, Tezpur University after surface modification. ATR FTIR spectra were recorded using a Nicolet Impact I-410 Spectrometer, Department of Chemistry, Tezpur University. Contact angle measurement before and after plasma treatment were carried out using contact angle measurement system from Data physics instrument GmbH, Germany, model OCA 15 EC at Department of Physics, Tezpur University. Contact angles of two polar liquids: water and ethylene glycol and a non-polar liquid: diiodomethane, were measured using sessile drop method on PAni nanofibers/Chitosan nanocomposites films before and after modification at room temperature. Contact angle data were recorded three times for each liquid and here, the averages of those have been presented with S.D. Absorbance data were acquired during Alamar blue assay using plate reader from Multiskan™ GO, Thermo Scientific, USA at Department of MBBT, Tezpur University.

Synthesis of Polyaniline (PAni) nanofibers

PAni nanofibers were synthesized using dilute polymerization method described by N. R. Chiou [36]. Briefly solution of 1M HCl (dopant acid) was prepared and the monomer aniline was dissolved in a small portion of that solution. Ammonium peroxydisulfate (oxidizing agent) was dissolved in the remaining portion of the dopant acid solution. The initial concentration of aniline in the reaction mixture was kept at 8 mM and the molar ratio of the monomer to the oxidant was maintained at 2:1. The monomer solution was then carefully transferred to the solution of APS. The reaction was allowed to take place in a magnetic stirrer at a very slow stirring rate at room temperature for about 24 h till the whole mixture became dark green. The whole mixture was then filtered and washed with deionized water and methanol for several times. For the purpose of film preparation, emeraldine base (EB) form of PAni has been obtained by further washing the mixture by 15% ammonia solution followed by several times with deionized water until the filtrate became colorless.

Synthesis of Polyaniline nanofibers/chitosan nanocomposites

Chitosan solution is prepared in 2 % (v/v) acetic acid solution. PAni nanofibers is added to chitosan solution at a concentration of 4% (w/v) and ultra-sonicated the mixture for one hour. The resultant solution is then casted on glass slide using a pasteur pipette and dried at 60°-70°C for 4 hours. After that films are removed by immersing the glass slides in water for 5-10 minutes.

Surface modification of Polyaniline (PAni) nanofibers/chitosan nanocomposites by gas plasma treatment

Surface modification of PAni nanofibers/Chitosan nanocomposites by plasma treatment was carried out in a stainless steel horizontal cylindrical chamber of

30 cm diameter and 100 cm length. The pressure inside the vacuum chamber is maintained at 1×10^{-3} mbar using a rotary pump and measured by a capacitance manometer. O_2, N_2 and Ar gases (purity > 99.9%) are separately fed into the vacuum chamber through a flat cylindrical gas shower plate and the flow rate of each gas is monitored by mass flow controller. The sample is placed on the surface of the RF electrode and the particular gas (O_2, N_2 or Ar) is introduced into the chamber. Uniform and stable plasma discharge is obtained using an RF generator (Seren, 0–300 W, USA) that is connected to a water cooled RF electrode through an L-type matching network. In the present wok, surface treatment of PAni nanofibers/Chitosan nanocomposites was carried out for 5 minutes at RF power value of 5 W and working pressure of 2×10^{-1} mbar.

Surface energy calculations

Surface energy parameters including total surface energy of both the samples were calculated according to AB method of Van Oss–Chaudhury–Good theory [23, 37]as this method distinguishes the acid–base (AB) interactions as a component of the surface free energy as follows:

$$\left(\gamma_s^{LW}\gamma_l^{LW}\right)^{0.5} + \left(\gamma_s^{+}\gamma_l^{-}\right)^{0.5} + \left(\gamma_s^{-}\gamma_l^{+}\right)^{0.5} = 0.5\gamma_l(1+\cos\theta) \tag{1}$$

$$\gamma_s^{LW} + \gamma_s^{AB} = \gamma_s \tag{2}$$

$$\gamma_s^{AB} = 2\left(\gamma_s^{+}\gamma_s^{-}\right)^{0.5} \tag{3}$$

where γ_s^{LW} and γ_l^{LW} =surface energy corresponding to Lifshitz–Van der Waals forces or dispersive components of solid and liquid respectively; γ_s^{+} and γ_l^{+} = Lewis acid components of solid and liquid respectively; γ_s^{-} and γ_l^{-} = Lewis base components of solid and liquid respectively; γ_s^{AB} =contribution of acid base interaction also refers to the polar component of solid surface.

It was performed by using contact angle data of three probe liquids: water ($\gamma^{LW} = 21.8\ \mathrm{mNm^{-1}}$, $\gamma^{+} = 25.5\ \mathrm{mNm^{-1}}, \gamma^{-} = 25.5\ \mathrm{mNm^{-1}}$), ethylene glycol ($\gamma^{LW} = 29\ \mathrm{mNm^{-1}}, \gamma^{+} = 1.92\ \mathrm{mNm^{-1}}$, $\gamma^{-} = 47.0\ \mathrm{mNm^{-1}}$ and diiodomethane ($\gamma^{LW} = 50.8\ \mathrm{mNm^{-1}}, \gamma^{+} = 0.01\ \mathrm{mNm^{-1}}, \gamma^{-} = 0$).

Results and discussion

Electron microscopy

The TEM images of PAni nanofibers are shown in **Fig. 1(a)**. The average diameter of PAni nanofibers is evaluated to be 35.66 nm from **Fig. 1(a)**. The SAED pattern [Inset of **Fig. 1(a)**] depicts two little intensified diffused rings indicating semicrystalline/crystalline phase of PAni nanofibers,

which is consistent with the inferences drawn from XRD analyses. Typical SEM micrographs of PAni nanofibers in powder form (**Fig. 1(b)**) demonstrate the nanofibrous structures of PAni with interconnected networks. The SEM micrographs of chitosan and PAni films are shown in **Fig. 2(a)** and **(b)**. **Fig. 2(a)** depicts homogeneous surface structure of chitosan film whereas surface structure with highly entangled aggregation among the nanofiber networks can be observed from the SEM micrograph of PAni film. The observed surface structure of PAni film has been confirmed from its stability in solution more than one day and is in agreement with earlier reports [26, 27]. The SEM micrographs of PAni nanofibers/ chitosan nanocomposite film [**Fig. 2(c)**] before plasma treatment appears to be layers of interconnected networks of PAni nanofibers soaked in chitosan matrix.
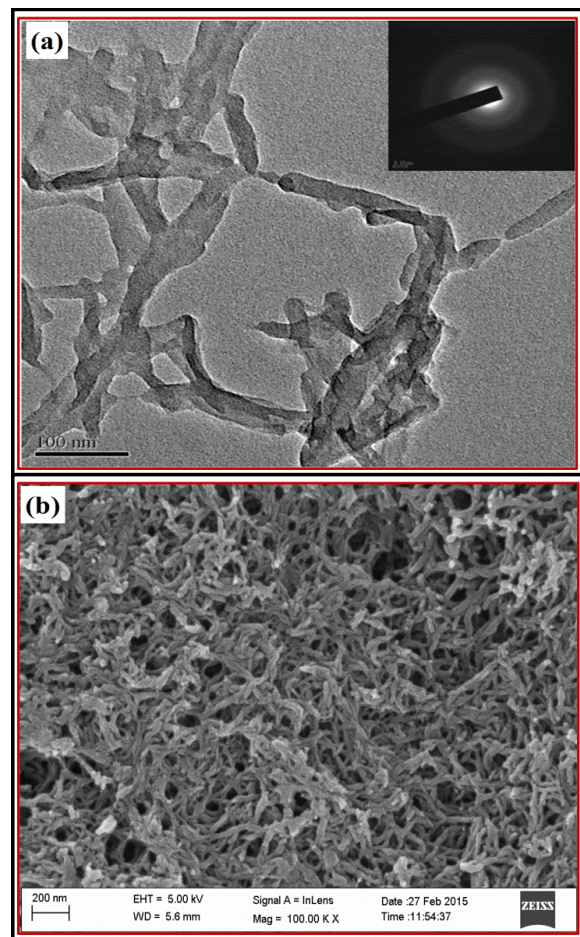

Fig. 1. (a) Transmission electron micrograph of PAni nanofibers. Inset shows SAED pattern of PAni nanofibers. (b) Scanning electron micrograph of PAni nanofibers in powder form.

The SEM micrographs of PAni nanofibers/Chitosan nanocomposite films after plasma treatment are shown in **Fig. 2 (d–f)**. As revealed from **Fig. 2(d)**, O_2 plasma treatment induces granular-like structures on the surface of PAni nanofibers/Chitosan nanocomposite film. N_2 plasma treated PAni nanofibers/Chitosan nanocomposite film

[**Fig. 2(e)**] shows stacked surface morphology with fewer defects than that observed in **Fig. 2(d)**. On the other hand, stacked surface along with distinct cavities is observed in Ar plasma treated PAni nanofibers/Chitosan nanocomposite film [**Fig. 2(f)**]. The findings thus reveal significant reactive ion etching on the surface of PAni nanofibers/Chitosan nanocomposite film induced by O_2 and N_2 plasma and dominant sputtering induced by Ar plasma. An enhanced surface roughness may be considered to have advantageous influence on cell adhesion and proliferation, felicitated by surface modification through plasma etching as well as sputtering [13].
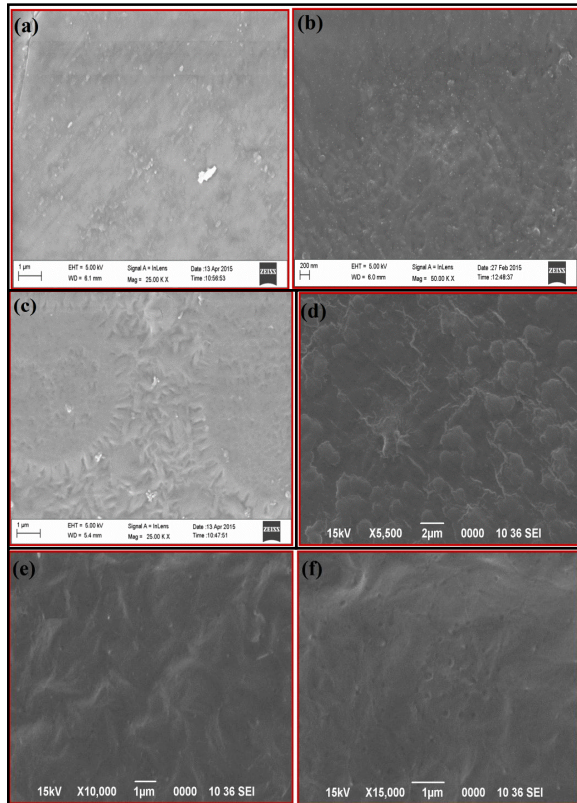

Fig. 2. Scanning electron micrographs of (a) Chitosan, (b) PAni nanofibers, (c) PAni nanofibers/Chitosan nanocomposites before plasma treatment and after (d) O_2 plasma (e) N_2 plasma and (f) Ar plasma treatment.

X-ray diffraction

Fig. 3. XRD patterns of (a) PAni nanofibers/Chitosan nanocomposites before plasma treatment (black). Inset shows XRD patterns of Chitosan (black) and Polyaniline nanofibers (red). (b) Comparison of XRD pattern of PAni nanofibers/Chitosan nanocomposites before (black) and after O_2 plasma treatment (red), N_2 plasma treatment (blue) and Ar plasma treatment (purple).

The XRD pattern of Cs shown in inset depicts a broad hump at around 22° indicating amorphous structure of chitosan [38]. Two peaks at around 20° and 25° appearing in the XRD pattern of PAni (inset) are characteristics of its amorphous emeraldine base form [39]. The XRD pattern of PAni

nanofibers/Chitosan nanocomposites before plasma treatment shows two peaks at around 20° and 22° that can be attributed to the regular arrangement within the nanocomposites through strong intermolecular hydrogen bonding between amine groups of PAni and amino/hydroxyl groups of chitosan [38].
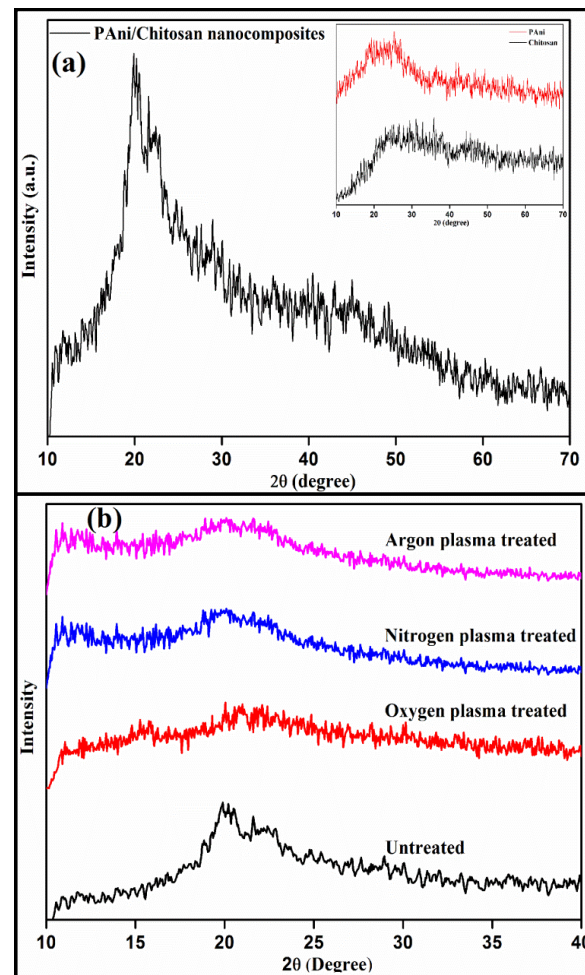

Fig. 3. XRD patterns of (a) PAni nanofibers/Chitosan nanocomposites before plasma treatment (black). Inset shows XRD patterns of Chitosan (black) and Polyaniline nanofibers (red). (b) Comparison of XRD pattern of PAni nanofibers/Chitosan nanocomposites before (black) and after O_2 plasma treatment (red), N_2 plasma treatment (blue) and Ar plasma treatment (purple).

The broadening of the above peaks in PAni nanofibers/Chitosan nanocomposites films after plasma treatment (**Fig. 3(b)**) can be attributed to dissociation of the intermolecular hydrogen bonds as well as dissociation and abstraction of weak bonds, due to bombardment of energetic ions that are generated in the plasma. The broadening of the peaks is more pronounced for the samples treated in O_2 plasma than that can be observed for samples treated in N_2 and Ar plasma. A shoulder peak appearing around 11° in the XRD patterns of PAni nanofibers/Chitosan nanocomposites after plasma treatment is originally a characteristic peak associated with chitosan. The appearance of the peak may be attributed to formation of some new bonds

leading to growth of new crystalline regions in the nanocomposites as a result of plasma treatment. The higher amorphous nature of PAni nanofibers/Chitosan nanocomposites after plasma treatment can be well corroborated with the results obtained from SEM analyses.

ATR-FTIR Spectroscopy

Fig. 4(a) shows ATR-FTIR spectra of PAni nanofibers and chitosan depicting their characteristic bands. The peak at ~823 cm^{-1} is assigned to C-H out of plane bending vibration of para disubstituted benzene ring [40-43]. The appearance of band at ~1063 cm^{-1} is attributed to C-N stretching vibration of primary amine of PAni backbone [40-42]. The peaks corresponding to C-N stretching vibration in Q=B=Q unit and N-H bending in –NH$_2$ of PAni appears at ~1382 and ~1321 cm^{-1}, respectively [40-43]. The vibrational bands in the region ~1450-1506 cm^{-1} and ~1595 cm^{-1} are associated with C=C stretching vibration of benzenoid and quinoid unit of PAni backbone [40, 41]. C=N stretching vibration in quinoid unit of PAni often overlaps in this region [43]. The broad vibrational band centered at ~3436 cm^{-1} is assigned to N-H stretching vibration [40, 43].

The appearance of the peak at ~1015 cm^{-1} in the ATR-FTIR spectrum of chitosan is assigned to O-H bending vibration [38]. The bands at ~1125 cm^{-1} and ~1260 cm^{-1} are attributed to anti-symmetrical stretching vibration of C-O-C bridge and C-N stretching vibration of secondary aromatic amine of chitosan, respectively [38]. A strong band at ~1630 cm^{-1} is assigned to C=O stretching in amide groups (-NHCOCH$_3$- due to partial deacetylation of Chitosan) [38]. Two weak bands appear at ~2855-2922 cm^{-1} is associated with C-H stretching of aliphatic group [38]. The broad band centered at ~3443 cm^{-1} is due to O-H & N-H stretching vibration in chitosan [38, 43].

The ATR-FTIR spectra of PAni/Chitosan nanocomposites before and after plasma treatment are shown in **Fig. 4(b)**. Characteristics vibrational bands for both PAni & chitosan are observed in PAni/Chitosan nanocomposites with shifting. After plasma treatment, the broadening and shifting of the band towards lower wavenumber region (~3420-3440 cm^{-1}) can be assigned to electrostatic forces & the hydrogen bonding between –OH & -NH$_2$ in PAni nanofibers/Chitosan nanocomposites. After O$_2$ plasma treatment, a small peak appears at ~1708 cm^{-1} due to stretching of C=O in carboxylic acid [43]. The peak may also be assigned to C=O in aldehyde, which moves to lower frequency. After N$_2$ plasma treatment, a broad peak appears in the region ~1620-1646 cm^{-1} which is attributed to C=N stretching vibration overlapped with C=O stretching vibration in amide groups of Chitosan [38,43]. The vibrational band associated with C-N stretching in secondary aromatic amine appearing at ~1254 for untreated sample shifts to ~1249, ~1254 and ~1260 cm^{-1} after O$_2$, N$_2$ and Ar plasma treatment, respectively. The C=C stretching vibration in quinoid/benzenoid unit observed at ~1506 cm^{-1} for untreated sample shifts to ~1546, 1551 and 1548 cm^{-1} after O$_2$, N$_2$ and Ar plasma treatment, respectively. The C-H out of plane bending vibration of para disubstituted benzene ring in PAni shifts to higher wavenumber from 823 cm^{-1} in PAni to 846, 895, 895 & 896 cm^{-1} for untreated, O$_2$, N$_2$ and Ar plasma treated samples, respectively. A very weak signature peak at 3440 cm^{-1} is observed after N$_2$ and Ar plasma treatment overlapped with the broad peak in the region 3220-3440 cm^{-1}.

As revealed from **Fig. 4(b)**, O$_2$ plasma treatment results in incorporation of oxygen containing functional groups (-OH, -CHO, -COOH etc.) onto the surface of PAni nanofibers/chitosan nanocomposite film. A possible mechanism showing generation of active sites induced by O$_2$ plasma and incorporation of functional groups onto the surface of PAni nanofibers/Chitosan nanocomposite film has been proposed and presented in **Fig. 5** and **Fig. 6**. The active sites 1 and 2 are exposed and accessible to highly reactive O$_2$ ions with the surface molecules which subsequently leads to incorporation of oxygen containing functional groups onto the polymer
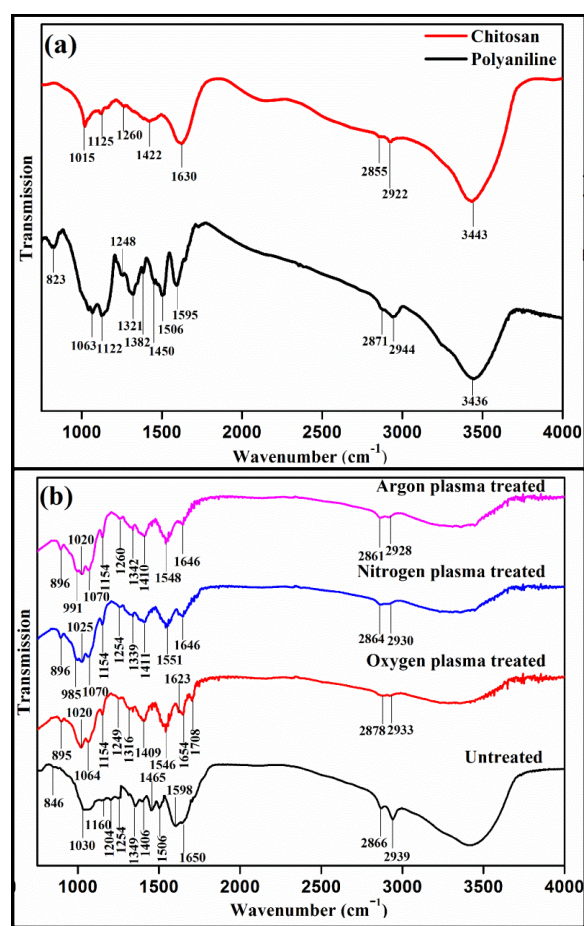
Fig. 4. (a)ATR-FTIR spectra of PAni nanofibers (black) and Chitosan (red). (b) ATR-FTIR spectra of untreated (black), O$_2$ plasma treated (red), N$_2$ plasma treated (blue) and Ar plasma treated (purple) PAni nanofibers/Chitosan nanocomposites.

surface. The reaction with the surface molecules of PAni nanofibers/Chitosan nanocomposite film by O_2 ions can proceed through a variety of mechanisms including abstraction, addition to unsaturated moieties etc., as shown in Scheme I of **Fig. 6**. In a similar way, reactive N_2 ions generated in N_2 plasma can participate in C-H bond cleavage and reacts with radical site of the polymer surface thereby introducing amine functional groups onto the surface as shown in Scheme II of **Fig. 6**. Unlike etching effect induced by O_2 and N_2 plasmas, Ar plasma treatment results in sputtering of the surface of PAni nanofibers/Chitosan nanocomposite film. Sputtering due to energetic ion bombardment leads to chain scission of the polymer molecules through hydrogen and carbon abstraction thereby generating free radicals on the surface. These free radicals when exposed to atmosphere readily react with atmospheric O_2 and/or water vapor which subsequently lead to incorporation of O_2 containing functional groups onto the surface of PAni nanofibers/chitosan nanocomposite film. The shifting of several vibrational bands as discussed earlier after Ar plasma treatment suggests the physical removal of molecules of fragments or breaking of bonds in the active sites of the polymer through chain scission and degradation processes of low molecular weight elements [**18**].
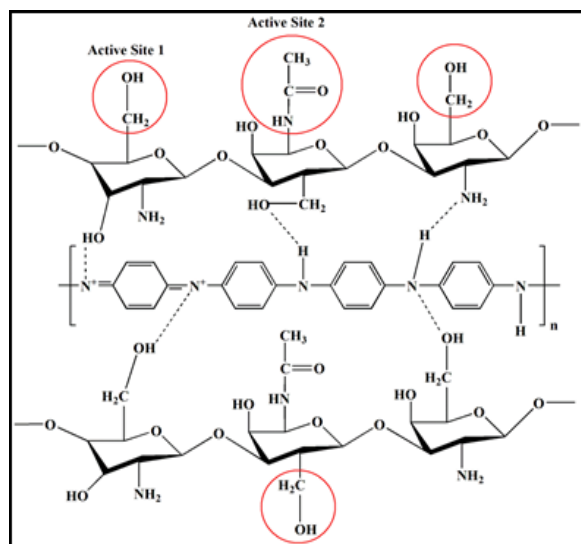
reaction of atomic O_2 with a polymer surface (active site 1 & 2 shown in **Fig. 5**), which is the starting point for the etching process. Attack of a polymer by atomic O_2 can proceed through a variety of mechanisms including abstraction, addition to unsaturated moieties etc. [Scheme I in **Fig. (6)**] [**18**]. Similarly, during N_2 plasma treatment atomic N participate C-H bond cleavage and further reactions of N with the radical site of the polymer surface introduce amine functionality to it [Scheme II in **Fig. 6**]. Compared to chemical etching, etching through sputtering is generally slow. During Ar plasma treatment, Chain scission generally occurs due to hydrogen & carbon abstraction leaving free radicals on the surface [**18, 44, 45**]. In the present work, Ar plasma treated samples were not exposed to atmosphere. Moreover, Ar is an inert gas and it can't directly incorporate functional groups unless exposed to atmosphere. There are no evidences of the presence of functional groups on the surface after Ar plasma treatment unlike after the O_2 and N_2 plasma treatment. The shifting of several vibrational bands as discussed earlier after Ar plasma treatment suggests the physical removal of molecules of fragments or breaking of bonds in the active sites of the polymer through chain scission and degradation processes of low molecular weight elements [**44, 45**].
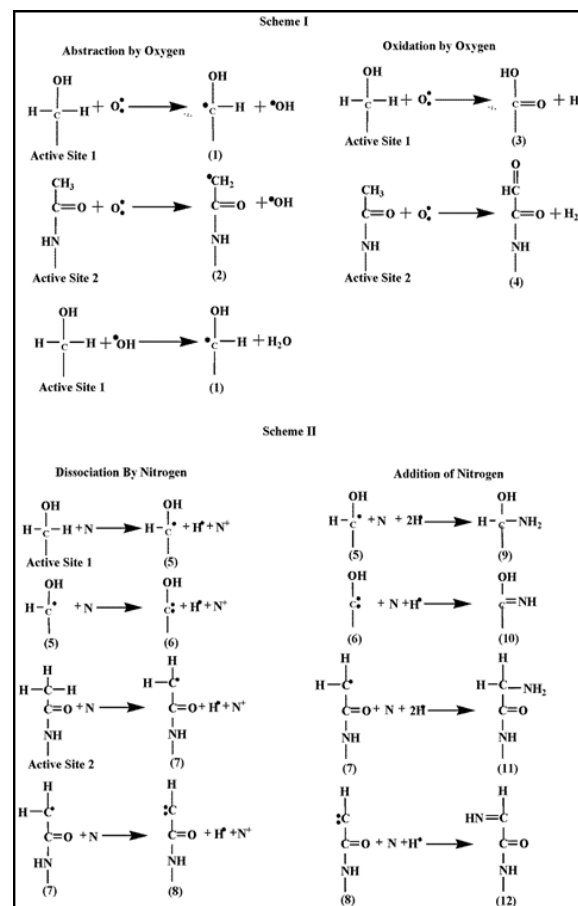

Fig. 5. Predicted chemical structure of PAni nanofibers/Chitosan nanocomposites showing active sites during plasma treatment.

During O_2 and N_2 plasma treatment, etching process dominates, while during Ar plasma treatment, sputtering process is more favorable. In O_2 plasma, atomic oxygen is the plasma species, while in N_2 plasma, plasma species are N_2 (Ground & Excited) and atomic N (N^+ is also formed during plasma treatment). ATR-FTIR results suggest incorporation of hydroxyl (-OH), aldehyde (-CHO) and carboxylic (-COOH) functionality after O_2 plasma treatment. O_2 gas plasmas are known to be very reactive etchants. This reactivity is due to the

Fig. 6. Probable chemical reactions and incorporation of polar functionality during O_2 plasma treatment (Scheme I) and N_2 plasma treatment.

Contact angle measurement

Surface modification by plasma treatment enhances the surface energy of Polyaniline nanofibers/Chitosan nanocomposites, which plays a key role in interfacial interactions between cell and the biomaterial [47,48]. Increase in Lewis basicity or basic component of surface energy calculated by AB method, is observed after plasma treatment, which is also a key factor for surface biocompatibility [49].

Table. I. Average Contact angle values for PAni nanofibers/Chitosan nanocomposites films before plasma treatment.

Material	Water Contact angle (°)	Ethylene Glycol Contact angle (°)	Diiodomethane Contact angle (°)
Untreated	73±0.07	62±0.22	47±0.07
Oxygen treated	43±0.10	48±0.01	52±0.17
Nitrogen treated	55±0.04	52±0.03	50±0.19
Argon treated	54±0.06	57±0.12	50±0.13

Table. II. Average surface energy and its components calculated by AB (water, ethylene glycol and diiodomethane) methods before plasma treatment.

Material	AB method				
	γ_s/mN m^{-1}	γ^{LW}_s/m Nm^{-1}	γ^{AB}_s/m Nm^{-1}	γ^+_s/m Nm^{-1}	γ_s/mNm^{-1}
Untreated	45.59±0.43	39.14±0.50	6.44	2.79±0.75	3.72±0.41
O$_2$ treated	52.71±0.30	38.39±0.67	14.31	3.09±0.25	16.57±0.44
N$_2$ treated	48.68±0.54	38.88±0.38	9.80	2.81±0.21	8.55±0.61
Ar treated	50.23±0.14	41.79±0.53	8.43	5.79±0.35	3.07±0.12

It was addressed earlier that surface properties of a material like wettability which is an important phenomenon for binding or adherence between two materials, can be evaluated by calculating surface energy of that material using contact angle values of different polar and apolar test liquids on it. Usually, the high energy surfaces due to nature of the chemical bonds (viz. covalent, ionic) hold them together, possess higher wettability. Thus, the presence of chemical groups on the surface of a material defines the wettability, which is one of the most prerequisite parameters for cell-biomaterial interfacial interactions. So far as, we have demonstrated directly the incorporation polar functional groups onto the surface of PAni nanofibers/Chitosan nanocomposites after O$_2$ and N$_2$ plasma treatment with the help of ATR-FTIR spectroscopy, there are no such direct method to calculate the total surface energy or surface tension except some indirect or semi-empirical methods. The Van Oss-Chaudhury-Good method, also known as Acid Base (AB) method offers the advantage over others in the sense that it can provide a complete scenario along with acidic and basic character of the surface beyond the total surface energy and dispersive and polar components.

Water contact angle values of PAni nanofibers/Chitosan nanocomposites before and after plasma surface modification with three different test liquids are shown in Table I. Decrease in water contact angle value upto 43°, 55° and 54° after O$_2$, N$_2$ and Ar plasma treatment, respectively, reveals the improved wettability of the material surface.

Surface energy calculations of PAni nanofibers/Chitosan nanocomposites before and after plasma treatment are performed by AB method using three test liquids: water, ethylene glycol and diiodomethane and presented in **Table I**. In fact, the "polar" term designate three classes of compound viz. hydrogen bonding compounds, dipolar compounds and the compounds that interact with Lewis acid and base.[23,49] This AB method reported by Van oss et al., distinguishes this acid base interactions as a component of surface energy denoted by γ^{AB}. As seen from Table II, the Lifshitz-Van der Waals components of PAni nanofibers/ Chitosan nanocomposites after O$_2$ and N$_2$ plasma treatment are significantly decreased to 38.39 and 38.88 mNm^{-1} from 39.14 mNm^{-1} observed before plasma treatment. But, the most important observation is the increase in acid-base components of surface energy after plasma treatment which ultimately leads to the improved hydrophilicity of the surface. It was found that γ^{AB}_s has been enhanced upto 14.31 and 9.80 mNm^{-1} from 6.44 mNm^{-1} after O$_2$ and N$_2$ plasma treatment. To speak more specifically, the Lewis base component (γ^-_s) of O$_2$ and N$_2$ plasma treated samples is enhanced by a large difference than that of untreated as observed from Table II, which indicates the improved basic character of plasma modified surface. The improved acid and basic character of the surface after Oxygen plasma treatment can be attributed due to the enrichment of the surface with carboxyl (-COOH) and hydroxyl (-OH), aldehyde (-CHO) functionality as depicted in the probable chemical interactions of plasma species of atomic O$_2$ with the active site 1 & 2 of PAni nanofibers/Chitosan nanocomposites [Scheme I in **Fig. 6**]. Similarly, the improved basicity of the surface after N$_2$ plasma treatment is addressed due to the incorporation of amine (-NH$_2$) functionality as shown in the predicted chemical interactions between the atomic Nitrogen plasma species and the active site 1 & 2 of Polyaniline nanofibers/Chitosan nanocomposites [Scheme II in **Fig. 6**].

On the other hand, the enhancement in surface energy after Ar plasma treatment can be assigned due to the formation of radical sites on the surface leading to dangling bonds or unsaturation. There are no evidences of introduction of functional groups after Ar plasma treatment from ATR-FTIR results. The unsaturation caused by Ar plasma may be due to the formation of radical sites through carbon and

hydrogen abstraction making the surface highly reactive. The modified surface absorbs water more easily notably due to the improved reactivity of the surface, which may be the reason for enhanced wettability and surface energy.

The enhancement in total surface energy value along with polar components specifically Lewis base component value after surface functionalization is correlated to the improved biocompatibility of plasma treated samples in the following section.

Cell viability study

The Alamar Blue assay was used to compare cell proliferation on different biomaterials based on detection of metabolic activity of viable cells through reduction of Alamar Blue. **Fig. 7(b)** depicts improved viability of PBMC cells on O_2 and N_2 plasma treated samples than as compared to the untreated and Ar plasma treated samples. Similar observations are also made in case of HepG2 cells. In case of the both cell types, it has been found that proliferation proceeded more significantly on O_2 and N_2 plasma treated samples than as compared to tissue culture plate (TCP).
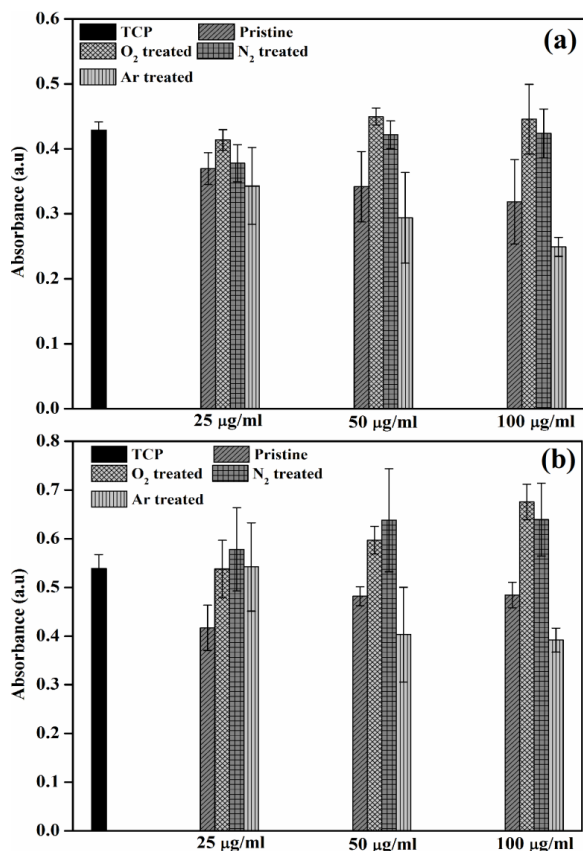

Fig. 7. Cell viability in terms of absorbance value of reduced form of Alamar Blue a function of sample concentration with (a) PBMC (Lymphocytes) and (b) HepG2 cells before and after plasma treatment. Absorbance data were recorded at 570 nm (experimental wells) and 600 nm (culture medium background as reference) and expressed as difference in absorbance at 570 nm and 600 nm ± SD for n = 4.

The optical micrographs of HepG2 cells on TCP, untreated and modified materials after 2 days of culture were shown in **Fig.S2** in the Supporting Information. It can be observed that O_2 and N_2 plasma treated samples demonstrate very good adherence towards Hep G2 cells [**Fig.S2(c) & (d)**], as the cells are nicely elongated on the surface. On the otherhand, less number of viable cells and no significant elongation of cells was observed on pristine and Ar plasma treated nanocomposites film [**Fig. S2(b) & (e)**]. These treatments appear to render the surface of PAni nanofibers/Chitosan nanocomposites with the appropriate physico-chemical properties for adherence and proliferation of Hep G2 cells.

The improved cell viability with both HepG2 and PBMC cells after O_2 and N_2 plasma treatment can be attributed to the enhanced surface hydrophilicity through introduction of polar functional like hydroxyl(-OH), aldehyde (-CHO), carboxyl (-COOH) and amine (-NH$_2$) functionality, as revealed from ATR-FTIR results and Surface energy calculations. The improved hydrophilic nature of PAni nanofibers/Chitosan nanocomposites after O_2 and N_2 plasma treatment enable it to interact with receptor proteins on the cell surface, which can mediate the cell growth along with other cellular activities. The reduced cell viability observed after Argon plasma treatment may be due to the creation of free radicals on the surface, which is generally considered as harmful to cells.

Conclusion

Plasma treatment comes out to be an effective technique for surface modification of PAni nanofibers/Chitosan nanocomposites. Scanning electron microscopy indicates increase in surface roughness due to etching during Oxygen and Nitrogen plasma treatment and due to sputtering during Argon plasma treatment. X-ray diffraction pattern shows broadening of the diffraction peaks around 19° & 25° after plasma treatment indicating increase in amorphocity of the nanocomposites. Surface hydrophilicity of PAni nanofibers/Chitosan nanocomposites has been successfully improved after Oxygen and Nitrogen plasma treatment through incorporation of polar functionality like hydroxyl (-OH), aldehyde (-CHO), carboxyl (-COOH) and amino (-NH$_2$) groups, respectively, as evident from ATR-FTIR and Contact angle measurements. Enhancement in wettability after plasma treatment is also supported by increase in surface roughness and amorphicity. Finally, O_2 and N_2 plasma treated samples are found to be more cytocompatible than the untreated and Argon plasma treated sample by Alamar Blue assay accomplished with Hep G2 cells and PBMC (Lymphocytes). Improved cell-biomaterial interaction is observed after O_2 and N_2 plasma treatment owing to its improved surface hydrophilicity, which mediates cell behaviour

through interaction with receptor proteins on cell surface. O_2 and N_2 plasma treated PAni nanofibers/Chitosan nanocomposites can act as artificial Extracellular Matrix (ECM) as they promote cellular activities and therefore, can be suitable biomaterial for various biomedical applications like tissue engineering, drug delivery and enzyme immobilization for biosensing applications. Improved bioactivity of PAni nanofibers/Chitosan nanocomposites after O_2 and N_2 plasma treatment towards Hep G2 cells may render them attractive as scaffolds for cancer cell growth for therapy and research, which may be an alternative to the conventional metal based technologies.

Acknowledgements

References

1. Ikada, Y.; *J. R. Soc. Interface,* **2006**, *3*, 589.
2. Ikada, Y.; Tissue engineering: fundamentals and applications; Academic Press: Belgium, **2011**.
3. Patrick, C. W.; Antonios, G. M.; McIntire, L. V. (Eds.); Frontiers in tissue engineering; Elsevier: USA, **1998**.
4. Vacanti, J. P.; Langer, R. *J.-Lancet,* **1999**, *354*, 32.
5. Spira, M.; Fissette, J.; Hal, C. W.; Hardy, S. B.; Gerow, F. J. *J. Biomed. Mater. Res.* **1969**, *3*, 213.
6. Giardino, R.; Aldini N. N.; Torricelli, P.; Fini, M; Giavaresi, G.; Rocca, M.; Martini, L.; *Int J Artif Organs,* **2000**, *23*, 331.
7. Ma, Z.; Kotaki, M.; Inai, R.; Ramakrishna, S. *Tissue Eng.* **2005**, *11*, 101.
8. Goldberg, M.; Langer, R.; Jia, X. *J. Biomater. Sci., Polym. Ed.* **2007**, *18*, 241.
9. Gentile, F.; Medda, R..; Cheng, L.; Battista, E.; Scopelliti, P. E.; Milani, P.; Cavalcanti-Adam, E. A.; Decuzzi, P. *Sci. Rep.* **2013**, *3*, 1461.
10. Lloyd, N.; Ncube, S.; Sibanda, P.; Akankwasa, N. T. *Mater. Sci.: Indian J.* **2012**, *12*, 218.
11. Webster, T. J.; Ejiofor, J. U. *Biomaterials*. **2004**, *25*, 4731.
12. Hosseinkhani, M.; Mehrabani, D.; Karimfar, M. H.; Bakhtiyari, S.; Manafi, A.; Shirazi, R. *World J. Plast. Surg.* **2014**, *3*, 3.
13. Sell, S. A.; Wolfe, P. S.; Garg, K.; McCool, J. M.; Rodriguez, I. A.; Bowlin, G. L. *Polymers*. **2010**, *2*, 522.
14. Balint, R.; Cassidy, N. J.; Cartmell, S. H. *Acta Biomater.* **2014**, *10*, 2341.
15. Ghasemi- Mobarakeh, L.; Prabhakaran, M. P.; Morshed, M.; Nasr- Esfahani, M. H.; Baharvand, H.; Kiani, S.; Al- Deyab S. S.; Ramakrishna, S. *J. Tissue Eng. Regener. Med.* **2011**, *5*, 17.
16. Ma, Z.; Mao, Z.; Gao, C. *Colloids Surf., B.* **2007**, *60*, 137.
17. Dai, L.; Mau, A. W. H. *J. Phys. Chem. B.* **2000**, *104*, 1891.
18. Olde Riekerink, M. B.; Structural and chemical modification of polymer surfaces by gas plasma etching; University Twente: Netherlands, **2001**.
19. Gomathi, N.; Neogi, S. *Appl. Surf. Sci.*, **2009**, *255*, 7590.
20. Svirachev, D. M.; Tabaliov, N. A. *Bulg. J. Phys.* **2005**, *321*, 22.
21. Castro Vidaurre, E. F.; Achete, C. A.; Gallo, F.; Garcia, D.; Simão, R.; Habert, A. C. *Mater. Res.* **2002**, *5*, 37.
22. Liston, E. M.; Martinu, L.; Wertheimer, M. R. *J. Adhes. Sci. Technol.* **1993**, *7*, 1091.
23. López-Pérez, P. M.; Marques, A. P.; da Silva, R. M.; Pashkuleva, I.; Reis, R. L. *J. Mater. Chem.* **2007**, *17*, 4064.
24. Oyane, A.; Uchida, M.; Yokoyama, Y.; Choong, C.; Triffitt, J.; Ito, A. *J. Biomed. Mater. Res., Part A.* **2005**, *75*, 138.
25. Kong, J. S.; Lee, D. J.; Kim, H. D. *J. Appl. Polym. Sci.* **2001**, *82*, 1677.
26. Kim, Y. J.; Kang, I. K.; Huh, M. W.; Yoon, S. C. *Biomaterials*, **2000**, *21*, 121.
27. Siow, K. S.; Britcher, L.; Kumar, S.; Griesser, H. J. *Plasma Processes Polym.* **2006**, *3*, 392.
28. Chen, M.; Zamora, P. O.; Som, P.; Peña, L. A.; Osaki, S. *J. Biomater. Sci., Polym. Ed.* **2003**, *14*, 917.
29. Mattioli-Belmonte, M.; Giavaresi, G.; Biagini, G.; Virgili, L.; Giacomini, M.; Fini, M.; Giantomassi, F.; Natali, D; Torricelli, P; Giardino, R. *Int. J. Artif. Organs*. **2003**, *26*, 1077.
30. Anderson, J. M. *Annu. Rev. Mater. Res.*, **2001**, *31*, 81.
31. Petrov, P.; Mokreva, P.; Kostov, I; Uzunova, V.; Tzoneva, R. *Carbohydr. Polym.* **2016**, *140*, 349.
32. Xu, D.; Fan, L.; Gao, L.; Xiong, Y.; Wang, Y.; Ye, Q.; Yu, A.; Dai, H.; Yin, Y.; Cai, J.; Zhang, L. *ACS Appl. Mater. Interfaces*, **2016**, *8*, 17090.
33. Miao, Z.; Wang, P.; Zhong, A.; Yang, M.; Xu, Q.; Hao, S.; Hu, X. *J. Electroanal. Chem.* **2015**, *756*, 153.
34. Pérez-Martínez, C.J.; Chávez, S.D.M.; del Castillo-Castro, T.; Ceniceros, T.E.L.; Castillo-Ortega, M.M.; Rodríguez-Félix, D.E.; Ruiz, J.C.G. *React. Funct. Polym.* **2016**, *100*, 12.
35. Min, Y.; Yang, Y.; Poojari, Y.; Liu, Y.; Wu, J.C.; Hansford, D.J.; Epstein, A.J. *Biomacromolecules*. **2013**, *14*, 1727.
36. Chiou, N. R.; Epstein, A. J. *Adv. Mater.* **2005**, *17*, 1679.
37. Van Oss, C. J; Roberts, M. J.; Good, R. J.; Chaudhury, M. K. *Colloids Surf.* **1987**, *23*, 369.
38. Ayad, M. M.; Salahuddin, N. A.; Minisy, I. M.; Amer, W. A. *Sens. Actuators, B*. **2014**, *202*, 144.
39. Pouget, J. P.; Jozefowicz, M. E.; Epstein, A. E. A.; Tang, X.; MacDiarmid, A. G. *Macromolecules*. **1991**, *24*, 779.
40. Furukawa, Y.; Ueda, F.; Hyodo, Y.; Harada, I.; Nakajima, T.; Kawagoe, T. *Macromolecules*. **1988**, *21*, 1297.
41. Sariciftci, N. S.; Kuzmany, H.; Neugebauer, H.; Neckel, A. *J. Chem. Phys.* **1990**, *92*, 4530.
42. Quillard, S.; Louarn, G.; Lefrant, S.; MacDiarmid, A. G. *Phys. Rev. B*. **1994**, *50*, 12496.
43. Pavia, D. L.; Lampman, G. M.; Kriz, G. E.; Introduction to spectroscopy; Thomson Learning: USA, **2008**.
44. Wagner, A. J.; Fairbrother, D. H.; Reniers, F. *Plasmas Polym.* **2003**, *8*, 119.
45. France, R. M.; Short, R. D. *Langmuir*. **1998**, *14*, 4827.
46. Wang, C.; Chen, J. R. *Appl. Surf. Sci.* **2007**, *253*, 4599.
47. Liu, L.; Chen, S.; Giachelli, C. M.; Ratner, B. D.; Jiang, S. *J. Biomed. Mater. Res., Part A*. **2005**, *74*, 23.
48. Kaelble, D. H.; Moacanin, J. *Polymer*. **1977**, *18*, 475.
49. Ostuni, E.; Chapman, R. G.; Holmlin, R. E.; Takayama, S.; Whitesides, G. M. *Langmuir*. **2001**, *17*, 5605.